EBioMedicine 21 (2017) 131–141

Contents lists available at ScienceDirect

EBioMedicine

journal homepage: www.ebiomedicine.com

Research Paper

A Critical Role of Zinc Importer AdcABC in Group A *Streptococcus*-Host Interactions During Infection and Its Implications for Vaccine Development

Nishanth Makthal [a], Kimberly Nguyen [a], Hackwon Do [a], Maire Gavagan [a], Pete Chandrangsu [b], John D. Helmann [b], Randall J. Olsen [a], Muthiah Kumaraswami [a,*]

[a] Center for Molecular and Translational Human Infectious Diseases Research, Houston Methodist Research Institute, Department of Pathology and Genomic Medicine, Houston Methodist Hospital, Houston, TX 77030, United States
[b] Department of Microbiology, Cornell University, Ithaca, NY 14853-8101, United States

ARTICLE INFO

Article history:
Received 10 January 2017
Received in revised form 30 May 2017
Accepted 31 May 2017
Available online 2 June 2017

Keywords:
Group A *streptococcus*
Host-pathogen interactions
Nutritional immunity
Gene regulation
GAS vaccine

ABSTRACT

Bacterial pathogens must overcome host immune mechanisms to acquire micronutrients for successful replication and infection. *Streptococcus pyogenes*, also known as group A streptococcus (GAS), is a human pathogen that causes a variety of clinical manifestations, and disease prevention is hampered by lack of a human GAS vaccine. Herein, we report that the mammalian host recruits calprotectin (CP) to GAS infection sites and retards bacterial growth by zinc limitation. However, a GAS-encoded zinc importer and a nuanced zinc sensor aid bacterial defense against CP-mediated growth inhibition and contribute to GAS virulence. Immunization of mice with the extracellular component of the zinc importer confers protection against systemic GAS challenge. Together, we identified a key early stage host-GAS interaction and translated that knowledge into a novel vaccine strategy against GAS infection. Furthermore, we provided evidence that a similar struggle for zinc may occur during other streptococcal infections, which raises the possibility of a broad-spectrum prophylactic strategy against multiple streptococcal pathogens.

1. Introduction

Nutrient acquisition by pathogens during infection is imperative for bacterial proliferation and disease development (Porcheron et al., 2016). The host exploits the nutritional requirements of the pathogen to limit growth by altering the availability of micronutrients at the colonization surface in a process referred to as nutritional immunity (Corbin et al., 2008; Damo et al., 2013; Kehl-Fie and Skaar, 2010; Ong et al., 2014). Although insights into the role of nutritional immunity in host defenses against pathogenic microorganisms are rapidly emerging (Corbin et al., 2008; Damo et al., 2013; Diaz-Ochoa et al., 2016; Gaddy et al., 2014; Haley et al., 2015; Hood et al., 2012; Liu et al., 2012), its involvement against several human pathogens, including group A *streptococcus* (GAS), is poorly understood. GAS is a versatile human-specific pathogen that colonizes different anatomic sites and causes diverse disease manifestations (Carapetis et al., 2005; Cunningham, 2000; Olsen et al., 2009). Furthermore, recurring and untreated infections can lead to post-infection immune-mediated complications such as rheumatic heart disease and post-streptococcal glomerulonephritis (Carapetis et al., 2016; Maurice, 2013; Rodriguez-Iturbe and Batsford, 2007). Given the morbidity and mortality associated with GAS infections, and the lack of clinically available prophylactic measures, identification of novel vaccine or antimicrobial targets to treat GAS infections is imperative (Carapetis et al., 2005; Carapetis et al., 2016; Sheel et al., 2016; Steer et al., 2016, 2013).

Zinc is an essential nutrient for microbial growth, but can be toxic in excess (Blencowe and Morby, 2003; Coleman, 1998). The delicate balance between zinc sufficiency and toxicity is maintained by bacterial metal homeostasis systems (Klaus, 2005; Moore and Helmann, 2005). The GAS metalloregulator, adhesin competence repressor (AdcR), regulates zinc homeostasis by monitoring the intracellular zinc concentration and modulating GAS adaptive response to zinc limitation (Sanson et al., 2015). During zinc sufficiency, the zinc-bound AdcR represses the expression of target genes, whereas the apo-AdcR relieves the repression during zinc deficiency. When cells encounter zinc limitation, GAS upregulates genes encoding zinc acquisition systems (*adcA, adcAII/lmb, adcBC, phtD*, and *phtY*), and zinc sparing responses (*rpsN.2* and *adh*) (Sanson et al., 2015). The primary GAS zinc uptake system, AdcABC, is composed of a cell surface-exposed zinc-binding protein (AdcA), an inner membrane permease (AdcB), and a cytosolic ATPase (AdcC) that provides the energy for zinc import by ATP hydrolysis. GAS also employs additional factors such as AdcAII/Lmb, PhtD, and PhtY to overcome zinc limitation (Sanson et al., 2015). Both AdcA and AdcAII share homologous N-terminal ZnuA-like extracellular zinc-binding domains. However, AdcA has an additional C-terminal ZinT-like

* Corresponding author.
E-mail address: mkumaraswami@houstonmethodist.org (M. Kumaraswami).

http://dx.doi.org/10.1016/j.ebiom.2017.05.030

domain and the role of the ZinT-like domain of AdcA in GAS homeostasis is yet to be elucidated. Although AdcAII/Lmb and Pht proteins contribute to streptococcal adaptive responses to zinc limitation (Bayle et al., 2011; Moulin et al., 2016; Tedde et al., 2016), the exact mechanisms by which they facilitate zinc acquisition remain unknown. Nevertheless, the significance of the AdcR signaling pathway to GAS pathogenesis is underscored by the observation that inactivation of *adcR* caused dysregulation of zinc homeostasis and significantly attenuated GAS virulence (Sanson et al., 2015).

The host recruits calprotectin (CP), an S100A8/A9 heterodimer, at microbial colonization surfaces and inhibits bacterial proliferation by sequestration of zinc, and manganese (Corbin et al., 2008; Damo et al., 2013; Diaz-Ochoa et al., 2016; Liu et al., 2012; Lusitani et al., 2003). The antibacterial activity of CP against bacterial and fungal pathogens has been demonstrated (Corbin et al., 2008; Damo et al., 2013; Diaz-Ochoa et al., 2016; Liu et al., 2012; Sohnle, et al., 1991; Urban, et al., 2009), but its role against most of the streptococcal pathogens is unknown. Emerging evidence indicates that GAS encounters host-mediated zinc immune mechanisms (Brenot et al., 2007; Ong et al., 2014). However, molecular details underlying host defense mechanisms, bacterial countermeasures, and their role in GAS pathogenesis are lacking. Using a multidisciplinary approach, we discovered that CP is a major host defense factor against GAS infection in different niches and mediates growth inhibition primarily by zinc sequestration. Conversely, GAS employs a high-affinity zinc uptake system and a refined sensory system to overcome CP-mediated growth inhibition. To realize the translational potential of our findings, we assessed and validated the extracellular component of the zinc importer, AdcA, as a potential GAS vaccine candidate.

2. Materials and Methods

2.1. Bacterial Strains, Plasmids and Growth Conditions

Bacterial strains and plasmids used in this study are listed in Supplementary Table S1. Strain MGAS10870 is representative of serotype M3 strains that cause invasive infections whose genome has been fully sequenced and has wild-type sequences for all major regulatory genes (Beres et al., 2010). Details of isogenic mutants construction using the parental serotype MGAS10870 is described in the Supplemental Experimental Procedures. *Escherichia coli* DH5α strain was used as the host for plasmid constructions and BL21(DE3) strain was used for recombinant protein overexpression. GAS was grown routinely on Trypticase Soy agar containing 5% sheep blood (BSA; Becton Dickinson) or in Todd-Hewitt broth containing 0.2% (w/v) yeast extract (THY; DIFCO). The *Escherichia coli* was grown in Luria-Bertani broth (LB broth; Fisher Scientific).

2.2. Animal Infection Studies

Mouse experiments were performed according to protocols approved by the Houston Methodist Hospital Research Institute Institutional Animal Care and Use Committee. These studies were carried out in strict accordance with the recommendations in the Guide for the Care and Use of Laboratory Animals, 8th edition. Mouse infections studies, analysis of colony-forming units (CFU), and histopathology of the infected tissues were carried out as detailed in the Supplemental Experimental Procedures.

2.3. Preparation of Total Protein Extracts From the Infected Tissues

To ensure that the CP levels measured are predominantly the secreted fraction, not the neutrophil cytosolic fraction, we employed methods to minimize contamination with intact neutrophils, neutrophil lysis, and acquisition of cytosolic CP. Typically, the abscess fluid is mostly acellular, and contains predominantly necrotized neutrophils. Intact neutrophils are likely to be around the edges of abscesses bordering with the healthy tissues and were not included in the sample preparation. The abscess fluid from the GAS infected tissues were carefully aspirated by puncturing the lesion and the purulent fluid was resuspended (30 mg of lesion/ml) in sterile PBS supplemented with a protease inhibitor cocktail pellet. Subsequently, the lesions were homogenized gently on ice and cell debris was removed by centrifugation at 20,000 $\times g$ for 30 min. The clarified supernatant was collected, filtered with 0.22 μm filter, and the total protein concentration was assessed by Bradford assay. The supernatant containing equal total protein concentration was assayed for CP by immunoblotting and ELISA assays.

2.4. Identification of Calprotectin in Infected Tissues by Immunoblotting

Equal concentrations of the total protein extracts from the tissue samples were resolved on a 15% SDS-PAGE gel, transferred to a nitrocellulose membrane, and probed with rat monoclonal anti-mouse S100A8, S100A9 (R&D Systems), and polyclonal anti-mouse GAPDH (Invitrogen) antibodies. Detection was accomplished by goat anti-rat secondary antibody conjugated with horseradish peroxidase (R&D Systems), and visualized by chemiluminescence.

2.5. Quantification of Calprotectin in Infected Tissues by ELISA

ELISA assays to measure calprotectin levels in the murine tissues were performed according to the manufacturer's instructions (Hycult Biotech). The calibration curve was generated using the calprotectin standard in the kit, and this curve was used to derive the concentration of calprotectin in the tissue samples. Samples were analyzed in triplicates and data were graphed as calprotectin concentration in micrograms per ml of total protein extract.

2.6. Bacterial Growth Studies in the Presence of CP

Recombinant human calprotectin was overexpressed and purified as detailed in Supplemental Experimental Procedures (Fig. S1). A 1:100 dilution of overnight GAS growth was inoculated into THY broth supplemented with calprotectin buffer (20 mM Tris pH 7.5, 0.1 M NaCl, 10 mM β-mercaptoethanol, 3 mM $CaCl_2$). The indicated concentrations of CP were added to the starter culture and growth was monitored by measuring A600 with a microplate reader. Samples were analyzed in triplicate and at least two different CP preparations were used.

2.7. Metal Content Analysis by Inductively Coupled Plasma Mass Spectrometry (ICP-MS)

Metal concentration in CP-treated growth medium, intracellular metal content of different GAS strains and variants of recombinant AdcR were analyzed by ICP-MS as described in Supplemental Experimental Procedures.

2.8. Transcript Level Analysis

GAS strains were grown to the indicated OD_{600} and incubated with two volumes of RNAprotect (Qiagen) for 10 min at room temperature. RNA isolation and purification were performed using an RNeasy kit (Qiagen). cDNA was synthesized from the purified RNA using Superscript III (Invitrogen) and Taqman quantitative RT-PCR was performed with an ABI 7500 Fast System (Applied Biosystems). Comparison of transcript levels was performed by the ΔC_T method of analysis using *tufA* as the endogenous control gene. The Taqman primers and probes used in this study are listed in Supplementary Table S2.

2.9. Overexpression and Purification of AdcR

The *adcR* gene of strain MGAS10870 was cloned into plasmid pET-21b and pET-15b. Protein overexpression and purification was performed as described previously and detailed in Supplemental Experimental Procedures.

2.10. Crystallization and Structure Determination of AdcR

Crystallization and structure determination of AdcR was performed by standard methods and detailed in the Supplemental Experimental Procedures.

2.11. Site-directed Mutagenesis of Recombinant AdcR

Plasmid pET21b-*adcR* or pDC-*adcR* containing the wild-type *adcR*-coding region was used as template for the site-directed mutagenesis. Quick change site-directed mutagenesis kit (Strategene) was used to introduce single amino acid substitutions within the *adcR* coding region and substitutions were confirmed by DNA sequencing. Mutant proteins were overexpressed and purified as described above.

2.12. Overexpression and Purification of AdcA-NTD

The coding sequence of the extracellular domain of *adcA* without the secretion signal sequence (amino acids 32-320) from strain MGAS10870 was amplified and cloned into *Nde*I and *Bam*HI restriction sites of *E. coli* overexpression vector pTYB21 (New England BioLabs). The details of AdcA-NTD purification is described in the Supplemental Experimental Procedures.

2.13. Mouse Immunization Studies

Female 3–4 week-old CD1 mice (Harlan Laboratories) were immunized with 10 μg of purified AdcA-NTD with either 2% aluminum hydroxide gel (Accurate Chemical and Scientific Corporation) or Sigma adjuvant system (Sigma-Aldrich) administered intramuscularly at 14, 28, and 42 days. The control group mice were immunized with either 2% aluminum hydroxide gel or Sigma adjuvant system mixed with PBS. Blood samples were collected after each round of immunization and the sera were separated.

2.14. Subcellular Fractionation of GAS Proteins

To maximize the expression of AdcA, chemically defined medium devoid of zinc was used for bacterial growth. GAS strains were grown to the late exponential growth phase (A_{600} ~ 1.0) and washed twice with PBS. Individual subcellular fractions of GAS growth were prepared as described in Supplemental Experimental Procedures. Equal concentration of the samples was probed for AdcA with anti-mouse AdcA serum by standard immunoblotting.

2.15. Western Immunoblotting Analysis

Purified AdcA-NTD was resolved by SDS-PAGE and transferred to nitrocellulose membranes. After blocking the membrane overnight with 4% nonfat milk, the membrane was incubated with mouse serum in TBS-T for 1 h at room temperature and rinsed with TBS-T for 15 min 3 times. The membrane was incubated for 1 h with goat anti–mouse horseradish peroxidase (HRP)–conjugated secondary antibodies diluted at 1:5000. Antibody-antigen interaction was visualized by chemiluminescence.

2.16. ELISA

To measure antibody titers of immune sera from mice vaccinated with recombinant AdcA-NTD, microtiter plates (Corning) were coated with purified recombinant AdcA-NTD at a concentration of 0.5 μg/ml and antibody levels in serum samples were determined using standard protocols. Plates were washed 3 times with TBS-T, and the uncoated surface was blocked with 2% skim milk (v/v) for 3 h at room temperature. The plate was incubated with serum from mock or immunized mice serially diluted 10-fold in TBS-T and incubated for 1 h at room temperature. Antigen-specific IgG was detected with HRP-conjugated secondary antibody and the plates were developed with TMB-Plus (Thermo Scientific) followed by addition of stop solution. Absorbance was measured at 450 nm, and the titer was determined as the dilution of immunized serum that was 3 times above the reading of the control (mock) serum.

2.17. GAS Challenge Studies

Immunized and control mice ($n = 20$) were challenged intraperitoneally with 5×10^7 CFU of GAS 2 or 5 weeks after the last immunization and monitored for near mortality using the parameters described in Supplemental Experimental Procedures. Results were graphically displayed as a Kaplan-Meier survival curve and analyzed using the log-rank test.

2.18. Detection of Human Antibodies Against AdcA

Blood was collected from patients with invasive GAS infections or no known recent GAS exposure (Streptolysin O negative). Samples were collected from patients with necrotizing fasciitis at the time of presentation to our hospital. Sera were separated by centrifugation and transferred to sterile cryovials for storage at −80 °C. This study was approved by the Institutional Review Board at Houston Methodist Hospital and Houston Methodist Research Institute.

Purified AdcA-NTD was resolved by SDS-PAGE and transferred to nitrocellulose membranes. The membrane was incubated with individual human serum sample at 1:50,000 dilution in TBS-T for 1 h at room temperature followed by additional 1 h incubation with goat anti-human HRP–conjugated secondary antibodies (Thermo scientific) diluted at 1:10,000. Antibody-antigen interaction was visualized by chemiluminescence.

3. Results

3.1. GAS Encounters Calprotectin During Infection

To investigate the role of CP in host defense against GAS infection, we assessed the presence of CP at GAS infection sites using two mouse models of invasive disease. Mice were infected either intramuscularly or subcutaneously with serotype M3 GAS or saline control and total protein extracts from the lesions were probed for CP by immunoblotting. CP was detected in intramuscular lesions from GAS-infected mice as early as day 1 post infection (pi) and this response persisted until day 4 pi (Fig. 1A). Furthermore, quantification of CP levels in the GAS-infected tissues by ELISA revealed that CP was present at an average concentration of ~61 μg/ml at day 1 pi and the levels increased significantly to 155 μg/ml at day 4 pi (Fig. 1B). Since GAS infects different host niches and the nutritional immune mechanisms vary with tissue microenvironment (Botella et al., 2011; Mason and Skaar, 2009; Ong et al., 2014), we also investigated the role of CP in a subcutaneous mouse model of invasive infection. As observed in intramuscular infection, CP was detected in GAS-infected tissues at an average concentration of 138 μg/ml at day 3 pi (Fig. 1C and D). Collectively, these results demonstrate that CP is present at GAS infection sites in the host and likely participates in host defense against GAS infection.

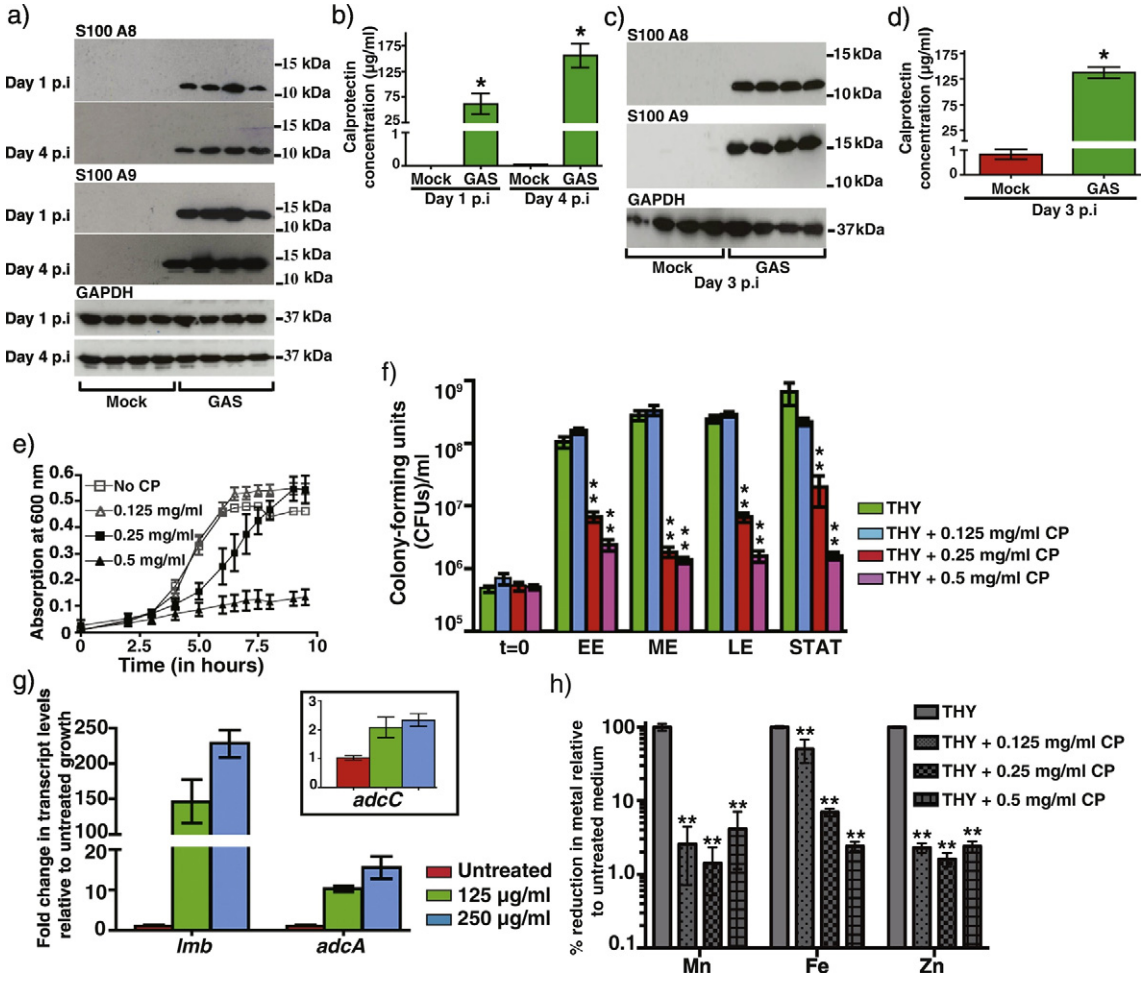

Fig. 1. Calprotectin is present at the GAS colonization surface in the host. a) Lesions from mice infected intramuscularly at days 1 and 4 post-infection with either saline (mock) ($n = 4$) or wild type GAS ($n = 4$) were probed for S100A8, S100A9, and loading control GAPDH by immunoblotting. b) Quantification of calprotectin in the infected muscular tissue lesions by ELISA. Data graphed are mean ± standard deviation. Statistical significance between the mock and GAS-infected samples is indicated by * ($P < 0.05$). *P* values were derived from two-sample *t*-test. c) and d) Calprotectin levels in the subcutaneous abscesses of mice infected with either saline (mock) ($n = 4$) or wild type GAS ($n = 4$) were analyzed by immunoblotting (c) and quantified by ELISA (d) at day 3 post infection. Data graphed are mean ± standard deviation. Statistical significance between the mock and GAS-infected samples is indicated by * ($P < 0.05$). *P* values were derived from two-sample *t*-test. e) GAS were grown in triplicate in THY broth supplemented with the indicated concentrations of CP. Growth was monitored by absorption at A_{600} in a microplate reader at the indicated time points. f) Comparison of the number of CFUs of GAS grown in the indicated concentrations of CP. Triplicate cultures were grown at the indicated conditions. Using the optical density of the untreated GAS growth, cells were collected at the start point ($t = 0$), early exponential (EE, A_{600} – 0.125), mid-exponential (ME, A_{600} – 0.25), late-exponential (LE, A_{600} – 0.375), and stationary (STAT, A_{600} – 0.5). Statistical significance between the untreated and calprotectin treated samples is indicated by ** ($P < 0.0001$). Data graphed are mean ± standard deviation. *P* values were derived from two-sample *t*-test. g) Transcript levels of *lmb, adcA,* and *adcC* in CP-treated GAS growth compared to untreated sample measured by qRT-PCR. Three biological replicates were grown and analyzed in triplicate. Data graphed are mean ± standard deviation. h) Metal content analysis of THY broth treated with the indicated concentrations of CP. Metal concentration (M) is denoted in the y-axis (in µM). Samples were analyzed in triplicate and data graphed are mean ± standard deviation. Statistical significance between the untreated and calprotectin treated samples is indicated by ** ($P < 0.0001$). *P* values were derived from two-sample *t*-test.

3.2. Zinc Sequestration by Calprotectin Contributes to GAS Growth Inhibition

To elucidate the role of CP in host defense against GAS infection, we purified recombinant human CP (CP) (Fig. S1) and tested bacterial growth at varying concentrations of CP. A CP concentration-dependent GAS growth inhibition was observed. GAS growth was comparable to untreated sample at the lowest CP concentration tested, whereas growth was either retarded (250 µg/ml) or inhibited at higher concentrations (500 µg/ml; Fig. 1E). The anti-streptococcal activity of CP was more evident in the colony-forming unit (CFU) analysis of GAS growth: it was drastically reduced at higher CP concentrations compared to the untreated control (Fig. 1F). However, GAS displayed a marked ability to sustain growth at 125 µg/ml and to a lesser extent at 250 µg/ml CP, suggesting that the pathogen possesses potent adaptive mechanisms to overcome CP-mediated bacteriostatic effect.

To elucidate the mechanism of growth inhibition by CP, we pursued two lines of investigation. To test whether CP imposes zinc starvation on GAS, we monitored the upregulation of AdcR-controlled genes as a marker for bacterial sensing of zinc limitation. Cells grown in the presence of 125 and 250 µg/ml of CP exhibited a dose-dependent induction of zinc acquisition systems (Fig. 1G). Transcript levels of the *lmb* gene were induced by ~146- and 228-fold at 125 and 250 µg/ml CP, respectively, relative to untreated control (Fig. 1G). A similar upregulation profile in concert with increasing CP concentration was observed for *adcA* and *adcC* genes (Fig. 1G). Subsequently, we measured zinc content in growth media treated with CP by ICP-MS. As expected, CP treatment significantly reduced zinc, manganese, and iron concentrations in the growth medium compared to untreated samples (Figs. 1H and S1E). Together, these results indicate that CP sequesters metal ions from GAS and induces a known zinc limitation response.

3.3. Zinc Uptake is Critical for GAS Defense Against CP and Pathogenesis

To understand the contribution of zinc importers to bacterial defense against host-mediated zinc sequestration, we constructed an isogenic Δ*adcC* mutant with an inactive cytoplasmic ATPase component of the tripartite zinc importer AdcABC (Fig. S2). Although Δ*adcC* mutant exhibited growth comparable to wild type (WT) in nutrient-rich medium, it displayed significant growth defects in either medium unamended with zinc or medium pretreated with zinc chelator, TPEN (Fig. 2A–C). Growth defect of the Δ*adcC* mutant was rescued by the *trans*-complementation plasmid *pDC-adcCB* (Figs. 2A–C, and S2). Furthermore, growth experiments with CP revealed an inability of Δ*adcC* to compete against CP-mediated zinc sequestration. Mutant growth was arrested at 125 μg/ml CP compared to 500 μg/ml CP required to cause similar effects on WT growth (Fig. 2D). Finally, metal content analysis of Δ*adcC* grown in rich laboratory medium revealed significant reduction in cytosolic zinc levels in the Δ*adcC* compared to WT and *trans*-complemented strains, indicating its critical role in zinc uptake by GAS (Fig. 2E). Collectively, these results underscore the significance of zinc uptake system in GAS defense against CP-mediated zinc limitation.

To determine the interplay between CP and bacterial zinc acquisition system *in vivo*, we compared the virulence of WT, Δ*adcC*, and *trans*-complemented strains using mouse models of necrotizing myositis and skin and soft tissue infection. In both models of invasive infection, virulence of Δ*adcC* was significantly attenuated compared to WT and *trans*-complemented strains (Fig. 2F–K). Histopathological analysis of

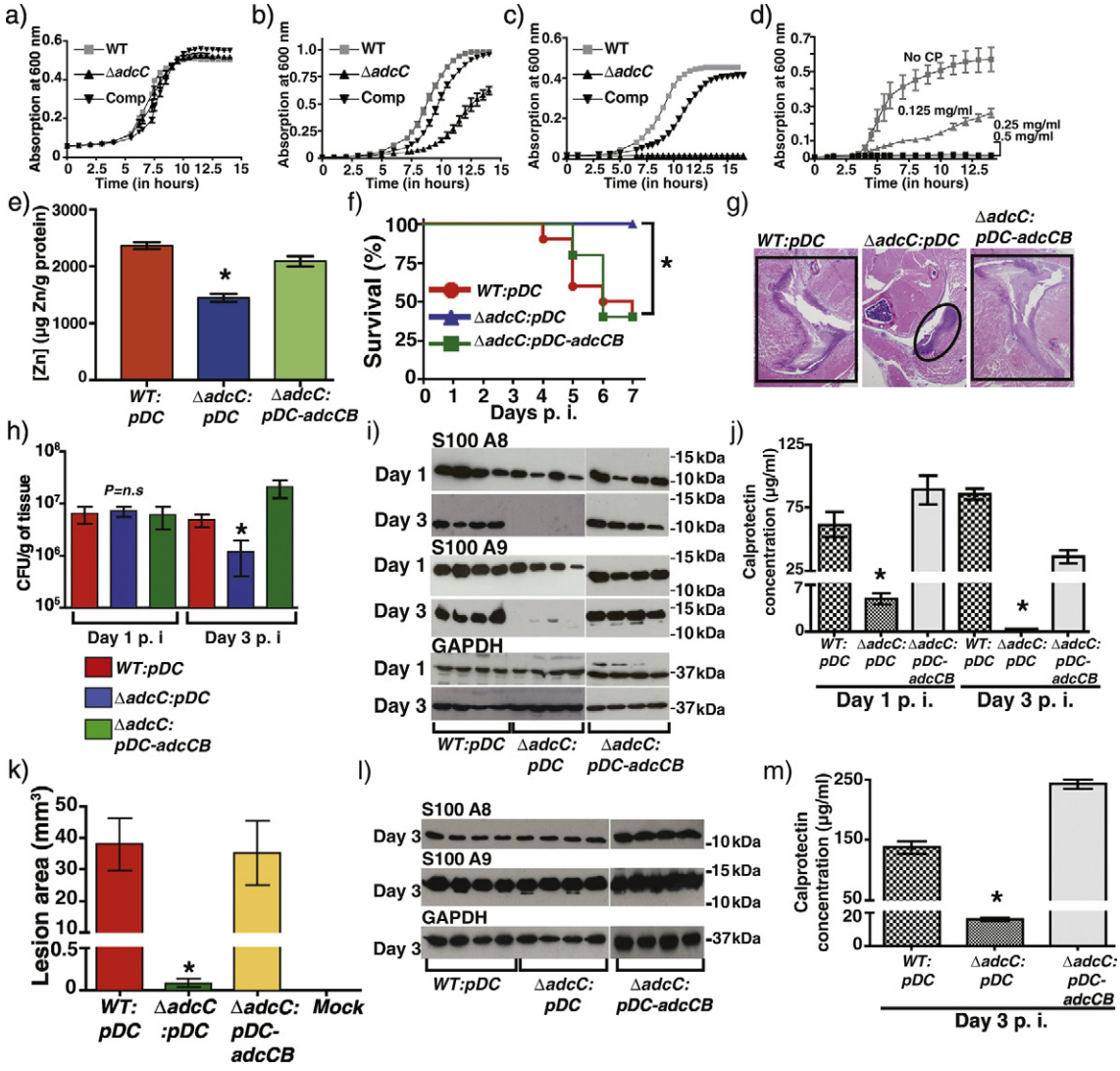

Fig. 2. Zinc limitation by calprotectin inhibits GAS growth. Growth curves of indicated strains in THY broth (a), chemically-defined medium devoid of zinc (b), and THY broth supplemented with 10 μM TPEN (c). d) The Δ*adcC* mutant was grown in triplicate in nutrient rich THY broth supplemented with the indicated CP concentrations. Growth was monitored by absorption at A_{600} in a microplate reader at the indicated time points. e) The WT, Δ*adcC*, and the *trans*-complemented strains were grown in THY broth and the intracellular metal content was measured by ICP-MS. Statistical significance between the WT, and Δ*adcC* mutant is indicated by * ($P < 0.05$). Data graphed are mean ± standard deviation. *P* values were derived from two-sample *t*-test. f) Ten outbred CD-1 mice per strain were injected intramuscularly with 1×10^7 CFU of each strain. Mouse survival depicted using a Kaplan-Meier curve with *P* values derived by log rank test. * indicates $P < 0.05$. g) Histopathological analysis of hindlimb lesions from mice infected with each indicated strain. Areas of host tissue damage are boxed, whereas confined, less destructive lesions are circled. h) Twenty mice were infected intramuscularly and mean CFUs recovered from the infected muscle tissue are shown with *P* value as determined by *t*-test. * indicates $P < 0.05$. Data graphed are mean ± standard deviation. i) Lesions from mice infected intramuscularly with the indicated strains were probed for S100A8, S100A9, and loading control GAPDH at days 1 and 3 post-infection by immunoblotting. j) Quantification of calprotectin concentration in the infected muscular tissue lesions by ELISA. Data graphed are mean ± standard deviation. Statistical significance between the WT, and Δ*adcC* mutant is indicated by * ($P < 0.05$). *P* values were derived from two-sample *t*-test. k) Ten immunocompetent hairless mice were infected with each indicated strain, and the lesion area produced by each strain was determined. Lesion area was measured day 3 p.i and graphed (mean ± standard error of the mean). *P* value was derived by log rank test. Statistical significance between the WT, and Δ*adcC* mutant is indicated by * ($P < 0.05$). l) Calprotectin levels in the subcutaneous abscesses of mice infected with the indicated strains were analyzed by immunoblotting (l) and quantified by ELISA (m). Statistical significance of $P < 0.05$ between the WT and Δ*adcC* mutant strain is indicated by *. Data graphed are mean ± standard deviation. *P* values were derived from two-sample *t*-test.

intramuscular lesions revealed that the Δ*adcC* caused markedly smaller lesions with less tissue destruction compared to WT and *trans*-complemented strains (Fig. 2G). Since *adcC* is critical for GAS survival *in vitro*, we assessed bacterial load in the infected muscular lesions by measuring CFUs. At day 1 pi, all 3 strains exhibited similar bacterial burden. However, consistent with *in vitro* findings, growth of Δ*adcC* was significantly reduced at day 3 pi, suggesting that the mutant has a decreased ability to survive *in vivo* (Fig. 2H). Measurement of CP levels revealed that lesions from mice infected with WT and *trans*-complemented strains had elevated levels of CP at both time points, whereas lesions caused by Δ*adcC* strain had much lower CP levels at day 1 pi and were significantly reduced at day 3 pi (Fig. 2I, and J). Similar observations were made in subcutaneous lesions (Fig. 2L and M), indicating that GAS adaptive responses to host-induced zinc limitation are critical for GAS pathogenesis at multiple host anatomic sites. These results also suggest that infection caused by Δ*adcC* mutant strain is resolved by host defenses earlier than WT and *trans*-complemented strains, leading to reduced inflammation and CP levels in lesions caused by Δ*adcC*. Together, these results emphasize the importance of the zinc uptake system to bacterial survival *in vivo* and GAS virulence.

3.4. Molecular Mechanism of Varied Gene Regulation by AdcR and Its Impact on GAS Virulence

GAS exhibited a dose-dependent induction of zinc acquisition genes in response to increasing CP concentration, which resembles our earlier findings that AdcR mediates gradual derepression of its target genes in response to decreasing zinc availability (Sanson et al., 2015). To deduce the molecular basis for varied gene regulation, we determined the crystal structure of AdcR. The AdcR dimer has a triangular-shaped fold, in which the DNA-binding and dimerization domains are located at the base and apex of the triangle, respectively (Figs. 3A and S3). Each AdcR subunit has one zinc atom bound at the interdomain region (Fig. 3A and B). Consistent with our previous genetic studies (Sanson et al., 2015), the zinc is coordinated by the side chains of H42 from helix α2, and H108 and H112 from helix α5 (Figs. 3B, and S3). Comparative structural analyses with the crystal structure of the related pneumococcal AdcR ($AdcR_{spn}$) (Guerra et al., 2011; Reyes-Caballero et al., 2010) revealed that the side chain of E24 from the loop connecting helices α1 and α2 also participate in zinc coordination. Due to the lack of well-defined electron density, we could not unambiguously locate the main chain and side chain atoms of E24 in $AdcR_{GAS}$ structure. Given that E24 is conserved between the two proteins, we hypothesized that the side chain of E24 is involved in zinc binding in $AdcR_{GAS}$. Furthermore, our X-ray analysis of AdcR crystals at the zinc absorption edge indicated that there are two zinc atoms per AdcR subunit within the asymmetric unit of AdcR crystal. Interestingly, the crystal structure of the $AdcR_{spn}$ has 2 zinc atoms per subunit (Guerra et al., 2011). The high affinity zinc site of $AdcR_{spn}$, site 1, corresponds to the site identified in $AdcR_{GAS}$ structure (Guerra et al., 2011). The second site in $AdcR_{spn}$, site 2, is coordinated by C30 from the loop connecting helices α1 and α2, E41 from helix α2, and E107 from helix α5 (Guerra et al., 2011; Reyes-Caballero et al., 2010) (Fig. S3). Importantly, the metal ligands identified at site 2 of $AdcR_{spn}$ are conserved in $AdcR_{GAS}$, suggesting that $AdcR_{GAS}$ may contain the analogous second zinc-sensing site. However, the second zinc could not be traced in the structure due to missing electron density for the loop connecting the helices α1 and α2 (Fig. S3).

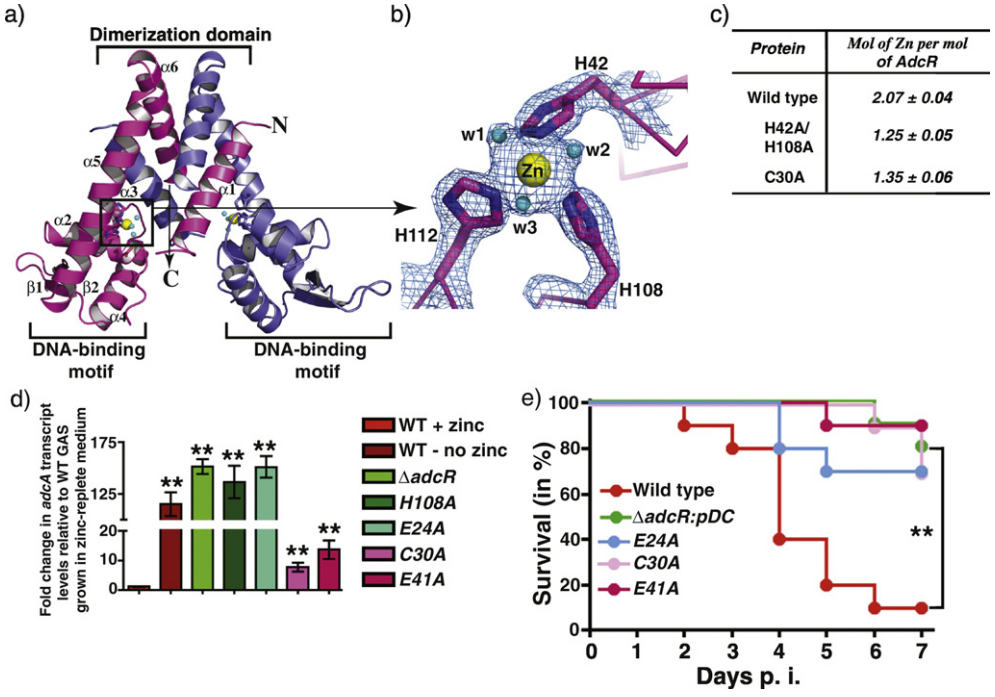

Fig. 3. Molecular mechanism of metal sensing and gene regulation by AdcR and its contribution to GAS pathogenesis. a) Ribbon representation of the crystal structure of AdcR dimer; individual subunits of a AdcR dimer are color-coded. The zinc atom bound to each AdcR subunit are shown as spheres and colored in yellow. The water molecules that participate in zinc coordination are shown as cyan spheres. The secondary structural elements of one subunit are labeled and the amino- and carboxy-terminus of the molecule are labeled as N and C, respectively. The DNA-binding and dimerization domains of AdcR are marked and labeled. b) A close up view of the metal-binding site (boxed in panel A) with the metal binding ligands labeled. Zinc bound to the primary metal sensing site in the structure of AdcR is shown as yellow sphere and the side chains of metal coordinating amino acids are depicted in stick representation. Water molecules are shown as cyan spheres. c) Metal content analysis of AdcR by ICP-MS. Measurements are reported as average from triplicate studies. Data shown are mean ± standard deviation. d) The indicated strains were grown to late exponential phase (A_{600} ~ 1.0) in zinc-replete chemically defined growth medium supplemented with 15 μM $ZnSO_4$ and transcript levels of *adcA* were measured by qRT-PCR. Three biological replicates were used. Data graphed are mean ± standard deviation. Average values for wild type strain grown in zinc-rich condition were used as reference and the fold changes in the transcript levels in the indicated strains relative to reference sample are shown above the bars. Statistical significance of $P < 0.0001$ between the reference and indicated mutant strains is indicated by **. *P* values were derived from two-sample *t*-test. e) Fifteen CD-1 mice were infected with each indicated strain intraperitoneally and the near mortality was presented on a Kaplan-Meier survival curve with *P*-values derived by log rank test. Statistical significance of $P < 0.0001$ is indicated by **.

To elucidate the regulatory roles of individual sites, we introduced single or double alanine substitutions at site 1 and site 2 metal ligands of AdcR. Since we have characterized the alanine mutants of metal ligand H42 and H108 at site 1 in our previous studies for DNA binding, gene regulation, and their contribution to GAS virulence (Sanson et al., 2015), we included the uncharacterized E24A mutant in this study. Similarly, to investigate the metal binding and gene regulation properties of site 2, we included the single alanine mutants of metal ligands C30 and E41 of site 2. To determine the metal content of AdcR, we purified recombinant WT AdcR and the alanine mutants of either site 1 (H42A/H108A) or 2 metal ligands (C30A). The purified WT and mutant AdcR proteins remained soluble and eluted as a dimer in the size exclusion chromatography, suggesting that the alanine substitutions did not cause major protein misfolding (data not shown). Next, we assessed the metal content of purified WT and mutant derivatives of AdcR by ICP-MS. The WT AdcR contains two zinc atoms per subunit (Fig. 3C), indicating the presence of two metal-sensing sites similar to $AdcR_{spn}$. However, the site 1 or 2 mutants have closer to one zinc per subunit (Fig. 3C), suggesting that AdcR can bind zinc independently at two different sites. To delineate the functional roles of AdcR metal binding sites, site 1 mutants (E24A and H108A), and site 2 mutants (C30A and E41A) were characterized for their regulatory function by qRT-PCR. In the absence of zinc, all tested strains displayed maximal induction of *adcA* expression (data not shown). However, 3 different phenotypes were observed in the presence of zinc. The fully metallated WT strain displayed the highest levels of repression, and site 1 mutants (E24A and H108A) and Δ*adcR* mutant exhibited a lack of repression. In contrast, site 2 mutants (C30A and E41A) displayed an intermediate phenotype, in which partial derepression was observed (Fig. 3D). These data indicate that zinc occupancy at site 2 has a role, albeit a lesser one, in regulating GAS adaptive response to zinc limitation. Since metal occupancy at site 1 is essential for gene regulation by AdcR but unnecessary for protein folding or dimerization (Guerra et al., 2011; Reyes-Caballero et al., 2010; Sanson et al., 2015), we designated this site as the primary metal-sensing site and site 2 as the secondary site. To corroborate the findings at the level of gene regulation to GAS pathogenesis, we assessed the virulence of WT, representative site 1 (E24A) and 2 (C30A and E41A) mutants using an intramuscular mouse model of infection. Results showed that virulence of site 1 or 2 mutants was significantly attenuated compared to WT, suggesting that both sites have functional roles *in vivo* and contribute significantly to GAS virulence (Fig. 3E).

3.5. Zinc Acquisition Machinery as a Prophylactic Target

Since the competition for zinc between GAS and the host occurs during the early stages of infection (Figs. 1 and 2), we hypothesized that targeting the bacterial zinc acquisition machinery may provide prophylactic opportunities to control GAS infections. Since AdcA is the extracellular component of the AdcABC transporter, we investigated whether AdcA might be a viable candidate for vaccine development. As antigen accessibility to the host immune system is a prerequisite for immunogenicity, we probed subcellular localization of AdcA in two GAS serotypes. AdcA was predominantly detected in the membrane and cytosolic fractions, indicating that AdcA is located on the bacterial surface (Fig. 4A). When lesions from the GAS-infected tissues were probed with anti-AdcA serum, AdcA was detected, confirming that AdcA is expressed in the host during infection (Fig. 4B). Subsequently, we tested immunogenicity of AdcA by vaccinating mice intramuscularly with purified recombinant AdcA N-terminal domain (AdcA-NTD, residues 36-320) mixed with either sigma adjuvant or clinically relevant alhydrogel, and testing the serum for reactivity (Figs. 4 and S4). Both adjuvants elicited significant antibody responses as serum from immunized mice displayed AdcA-specific reactivity and progressively higher titers after successive rounds of immunization (Figs. 4C–D, and S5). To correlate antibody titers with protection, immunized and control mice were challenged 2 weeks post final immunization by systemic GAS infection with fully sequenced clinical isolates belonging to serotypes M1, M3, M89, and M12 GAS. Mice immunized with AdcA conferred significant protection against all tested serotypes compared to the mock-treated group, indicating that AdcA is a potent vaccine antigen that affords immunity against GAS infection (Figs. 4E–H and S5). Similar protection was observed in challenge studies performed 4 weeks post final immunization with serotype M1 GAS, suggesting that AdcA vaccination confers sustained protection (Fig. 4I). Importantly, the level of protection observed with AdcA immunization is comparable to other tested GAS antigens including the leading GAS vaccine candidate, M protein (Dale et al., 2015; Kapur et al., 1994; McNamara et al., 2008; van Sorge et al., 2014; Zhang et al., 2006). Finally, we assessed immunological recognition of AdcA by human sera from patients with history of acute invasive GAS infections. Reactivity to AdcA was detected in the serum of all GAS-infected patients but not in serum from healthy controls with no recent history of GAS infection (Fig. 4J). This indicates that AdcA is accessible to host immune effectors and triggers antibody responses during natural infection in humans.

3.6. CP Inhibits the Growth of Pathogenic Streptococci

To investigate whether host-mediated zinc sequestration is a general conserved immune mechanism used against other pathogenic streptococci and *Listeria monocytogenes*, we performed growth studies of various streptococci and *L. monocytogenes* in the presence and absence of CP. As observed for GAS, CP inhibited the growth of all tested bacteria, albeit to a different extent (Fig. 5A–G). Notably, pneumococci displayed significant resistance against CP-mediated growth inhibition as the bacteria retained the ability to grow even at CP concentration of 500 μg/ml, whereas CP at the same concentration caused growth arrest of other streptococci and *L. monocytogenes* (Fig. 5E). Given that the amino acid sequence of the zinc acquisition machinery is highly conserved among the tested pathogens, it is likely that these pathogens employ uptake systems analogous to *adcABC* to acquire zinc and compete with host sequestration mechanisms (Fig. 5H). Thus, prophylactic targeting of zinc import machinery, as demonstrated in GAS, may be a viable broad-spectrum vaccine strategy against these important human pathogens.

4. Discussion

Molecular dialog between host and invading pathogens shapes the course of infection and often determines the disease outcome. We identified a previously unknown GAS-host interaction that occurs during infection and demonstrated that zinc is at the forefront of the host-GAS battle. Furthermore, we showed that the molecular arsenals of the pathogen involved in this host-pathogen conflict could be effectively targeted for disease prevention. Herein, we report that GAS-infected lesions are enriched with CP in two different host compartments and CP retards GAS growth by scavenging zinc from the colonization interface. Our results are consistent with the observations made in other bacterial pathogens including *S. aureus, A. baumannii, S. typhimurium*, and *H. pylori* (Gaddy et al., 2014; Hood et al., 2012; Corbin et al., 2008, Damo et al., 2013; Liu et al., 2012). In addition to zinc, CP also inhibits bacterial growth by sequestering manganese and iron (Damo et al., 2013; Diaz-Ochoa et al., 2016; Nakashige et al., 2015). Given that GAS adaptive responses to manganese limitation are not fully understood, the role of CP-mediated manganese sequestration on GAS pathogenesis is yet to be elucidated. Similarly, CP binds iron and causes bacterial growth inhibition *in vitro* (Nakashige et al., 2015), however, the *in vivo* significance of CP-mediated iron limitation as a host defense remains unclear (Garcia et al., 2017).

Although the role of CP against pneumococcal infection has been investigated, the two studies provided opposing findings with varying mechanisms for CP to either inhibit or facilitate pneumococcal virulence. One study reported that CP is an anti-pneumococcal host factor

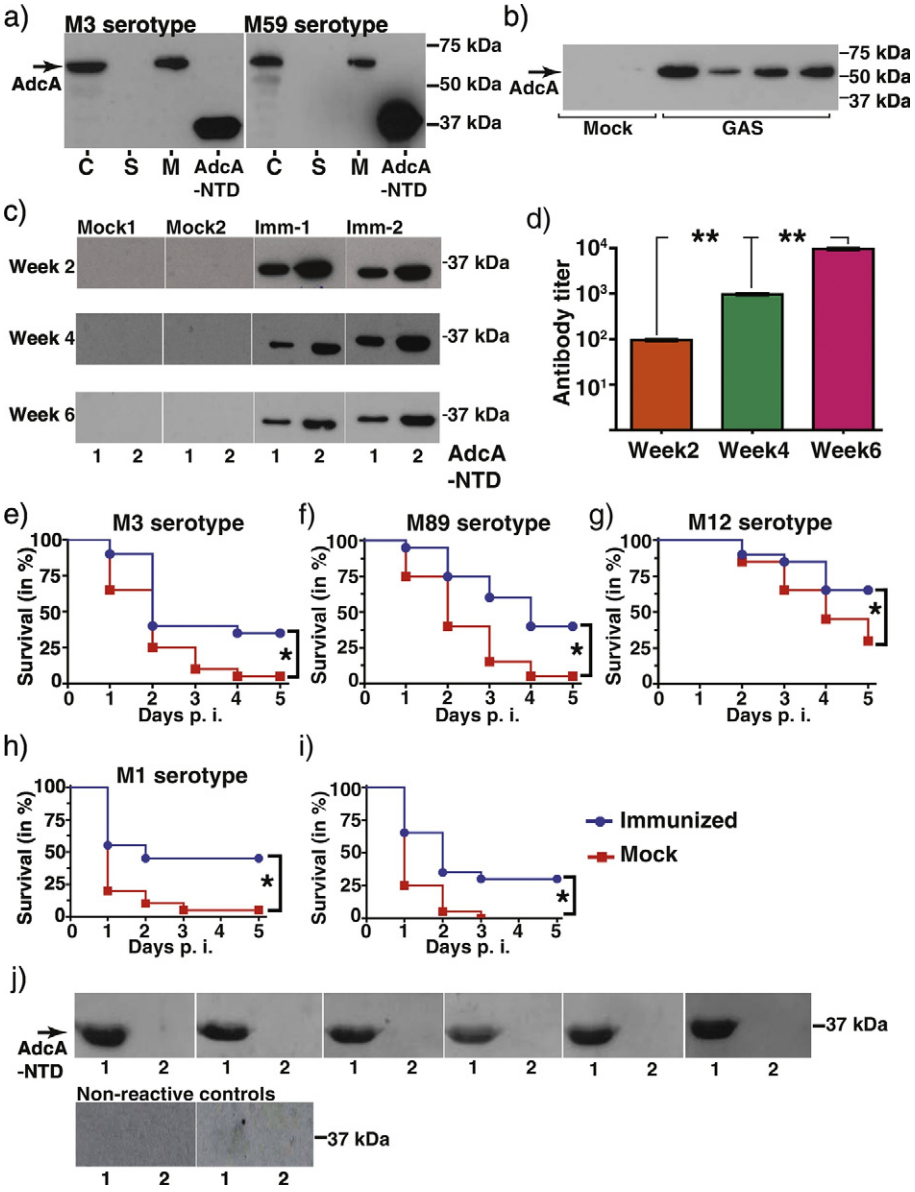

Fig. 4. AdcA is a potent vaccine candidate. a) Subcellular localization of AdcA. The cytosolic (C), secreted (S), and membrane (M) fractions of WT GAS grown to mid-exponential growth phase were isolated and probed for AdcA by western blotting. The recombinant N-terminal domain (NTD) of AdcA was used as positive control. Positions of molecular weight markers with their masses (kDa) are shown. b) AdcA is produced during infection. Protein extracts from the lesions from mice infected with either saline (mock) ($n = 2$) or WT GAS (GAS) ($n = 4$) were analyzed for AdcA by immunoblotting. c) Increasing concentrations of purified AdcA-NTD (lane 1–0.5 μg and lane 2–2 μg) were resolved by SDS-PAGE and transferred to nitrocellulose membrane. AdcA-NTD specific antibodies in serum from mice immunized intramuscularly with either 2% Aluminum hydroxide gel adjuvant (Accurate Chemical and Scientific Corporation) (mock) or AdcA-NTD mixed with 2% Aluminum hydroxide gel adjuvant (Accurate Chemical and Scientific Corporation) (Imm) at weeks 2-, 4-, and 6- post immunization were assessed by western blotting. d) Titers of AdcA-NTD specific antibodies in immunized mouse serum ($n = 6$ per group) measured by ELISA. Data graphed are mean ± standard deviation. Statistical significance of $P < 0.0001$ between the week 2 post immunization and weeks 4 and 6 post immunization samples is indicated by **. *P* values were derived from two-sample *t*-test. Immunization of mice with purified recombinant AdcA-NTD confers protection against lethal GAS infection. Kaplan-Meier survival curve of mice challenged intraperitoneally with GAS serotypes M3 (e), M89 (f), M12 (g), and M1 (h) 2 weeks after the final immunization with purified AdcA-NTD. Twenty mice per group were used for the challenge studies. Statistical significance of $P < 0.05$ between the mock and immunized group is indicated by *. i) Kaplan-Meier survival curve of mice challenged intraperitoneally with serotype M1 GAS 4 weeks after the final immunization with purified AdcA-NTD. Twenty mice per group were used for the challenge studies. Statistical significance denoted by *P*-values derived by log rank test. Statistical significance of $P < 0.05$ between the sham and immunized group is indicated by *. j) Immunoblot analysis of AdcA-NTD with human sera. Purified AdcA-NTD (lane 1) and cytosolic regulator RopB (lane 2) were resolved by SDS-PAGE and transferred to nitrocellulose membrane. Sera obtained from patients with invasive disease (top row) were used at 1:50,000 dilution for detection. Sera obtained from two different streptolysin O negative individuals were treated as non-reactive controls (bottom row), whereas purified cytosolic regulator RopB (lane 2) was used as a non-specific protein control.

that inhibits bacterial growth during infection (De Filippo, et al., 2014), whereas a second investigation suggested that CP facilitates bacterial infection (Achouiti, et al., 2014). Thus, additional investigations are required to elucidate the precise role of CP against pneumococcal infection. In this regard, results from this study provided significant evidence that GAS encounters CP-mediated Zn limitation during invasive infection and indicated similar susceptibility of other streptococcal pathogens to CP. The observations that CP is abundant at GAS infection sites, CP imposes Zn limitation on GAS, and adaptive responses to Zn starvation are highly upregulated during GAS invasive infections lend support to our findings (Brenot et al., 2007). However, it is likely that GAS may encounter additional nutritional immune mechanisms such as zinc toxicity in other host compartments during infection (Ong et al., 2014).

The GAS arsenals to combat CP-mediated zinc withholding include the high-affinity zinc importer, AdcABC and the zinc sensor, AdcR.

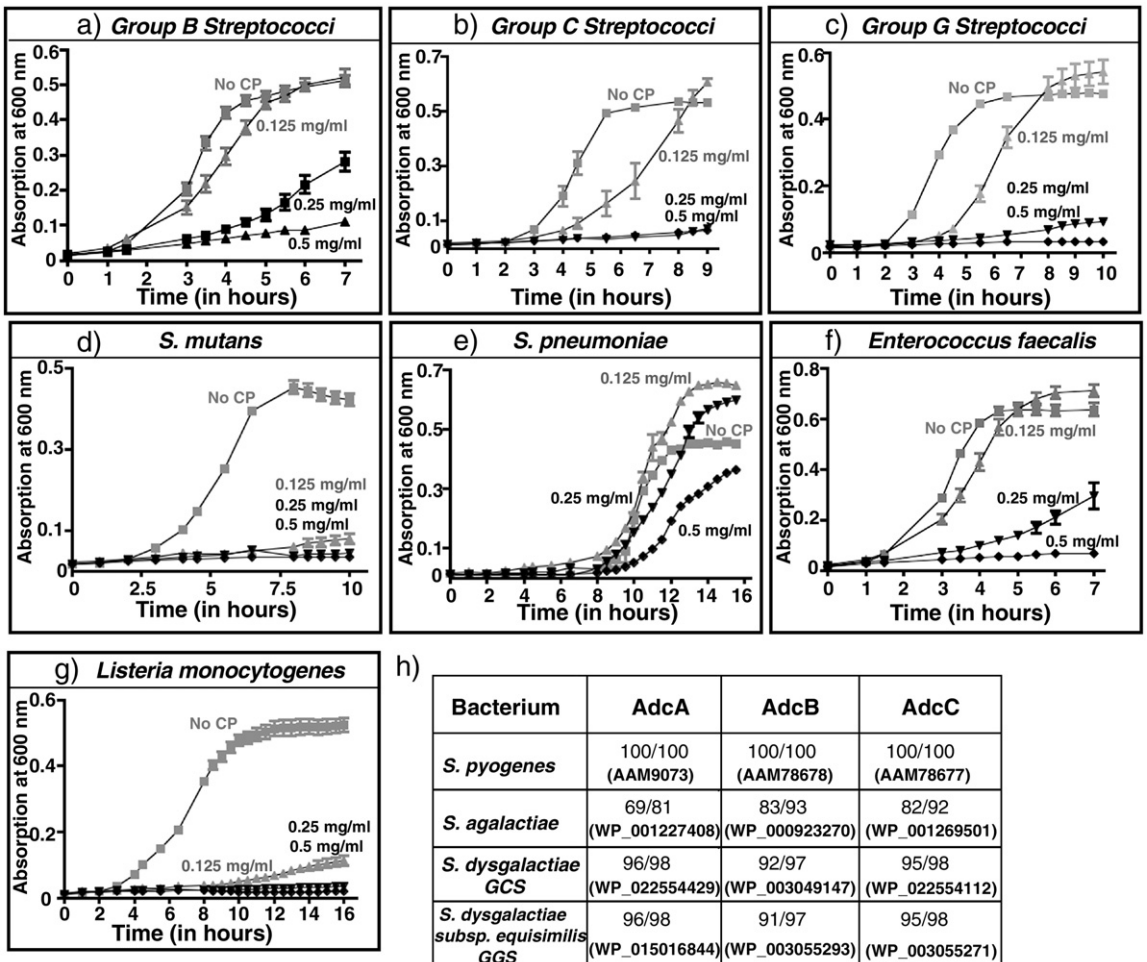

h)

Bacterium	AdcA	AdcB	AdcC
S. pyogenes	100/100 (AAM9073)	100/100 (AAM78678)	100/100 (AAM78677)
S. agalactiae	69/81 (WP_001227408)	83/93 (WP_000923270)	82/92 (WP_001269501)
S. dysgalactiae GCS	96/98 (WP_022554429)	92/97 (WP_003049147)	95/98 (WP_022554112)
S. dysgalactiae subsp. equisimilis GGS	96/98 (WP_015016844)	91/97 (WP_003055293)	95/98 (WP_003055271)
S. pneumoniae	62/76 (WP_057488132)	75/91 (WP_000950021)	78/89 (WP_050252568)
S. mutans	63/79 (WP_002268534)	81/92 (WP_002299867)	82/91 (WP_002263428)
E. faecalis	56/71 (WP_010820563)	61/83 (WP_005230272)	64/82 (WP_016624321)
L. monocytogenes	56/71 (WP_010825573)	55/76 (WP_031695371)	57/76 (WP_009917491)

Fig. 5. Broad-spectrum anti-streptococcal activity of calprotectin. Growth characteristics of streptococcal pathogens, a) group B *streptococcus* (*S. agalactiae*), b) group C *streptococcus* (*S. dysgalactiae*), c) group G *streptococcus* (*S. dysgalactiae* subsp. *equisimilis*), d) *S. mutans*, e) *S. pneumoniae*, f) *Enterococcus faecalis*, g) *Listeria monocytogenes*, was assessed. Bacteria were grown in triplicate in medium supplemented with the indicated concentrations of CP. Growth was monitored by absorption at A_{600} in a microplate reader at the indicated time points. h) Amino acid sequence conservation of AdcA, AdcB, and AdcC proteins among different streptococcal pathogens. The respective amino acid sequence identities and chemical similarities relative to GAS sequences are shown. The protein identification number of the respective proteins is given in parentheses.

Although several studies demonstrated the importance of metal importers to bacterial pathogenesis (Ammendola et al., 2007; Campoy et al., 2002; Davis et al., 2009; Bayle, et al., 2011; Sabri, et al., 2009), this study delineated the direct role of a zinc transporter in evading host nutritional immune defenses and highlighted its significant contribution to GAS survival during infection (Fig. 2). The *adcCB*-inactivated strain is unable to compete against CP due to defective zinc acquisition, which likely results in growth retardation and premature bacterial clearance from the site of infection. Consistent with this, Δ*adcC* mutant exhibited reduced *in vivo* survival and significantly attenuated virulence compared to WT and *trans*-complemented strains. Furthermore, GAS actively monitors alterations in zinc availability during infection and mounts a measured induction of adaptive responses that correlates with the degree of reduction in zinc concentration. AdcR employs two metal-sensing sites to monitor zinc availability, and each site has defined biological roles in gene regulation and GAS pathogenesis. Metallation of the primary zinc-sensing site is essential for AdcR-promoter interactions and transcription repression, and vacant site 1 results in full derepression of regulated genes. The secondary zinc-sensing site has a lesser regulatory role as zinc binding at this site causes tighter repression, and loss of zinc at site 2 leads to lower levels of target gene derepression. Such gradual gene regulation by AdcR may afford significant growth advantage as it allows the pathogen to sense and respond to broader range of alterations in zinc concentrations. CP levels are relatively low during early stages of infection, which likely imposes milder zinc limitation on the pathogen and requires lower level induction of GAS adaptive responses. As CP concentration increases during later stages of infection, a further drop in zinc concentration may necessitate robust induction of adaptive responses. Varied target gene regulation in response to altering zinc concentration has been observed in zinc metalloregulators, Zur from *B. subtilis* and *Streptomyces coelicolor*, and Zap1 from *Saccharomyces cerevisiae* (Ma et al., 2011; North et al., 2012; Shin et al., 2011; Shin and Helmann, 2016; Wu et al., 2008). However, this is the first study demonstrating the functional relevance of

gradual gene regulation by a metalloregulator to the virulence of a human pathogen.

Since the GAS-host confrontation for zinc occurs during early stages of infection and zinc acquisition systems are upregulated to disarm host defenses (Brenot et al., 2007), we hypothesized that bacterial zinc uptake machinery could be targeted as a protective vaccine against GAS infection. To probe this, we demonstrated that the extracellular component of zinc uptake system, AdcA, is expressed during infection, accessible on the bacterial surface, antigenic, and immunization with recombinant AdcA-NTD confers protection against systemic GAS infection (Fig. 4). Importantly, as a vaccine candidate, AdcA has the potential to overcome longstanding barriers in GAS vaccine research. AdcA is highly conserved and elicited protection against different tested GAS serotypes, thus increasing the likelihood of conferring protection across multiple GAS serotypes (Figs. 4, and S6). Structural modeling indicated the lack of coiled-coil structures in AdcA, as observed in M protein structures (Kirvan et al., 2014; McNamara et al., 2008), which minimizes the possibility for elicitation of autoimmune reactions against human cardiac tissues, the etiology behind rheumatic heart disease (Figs. S7 and S8). Finally, all the tested representatives of different groups of streptococci exhibited susceptibility to CP and encode structurally similar zinc acquisition machinery in their genomes (Figs. 5, and S8), suggesting that other streptococcal pathogens as well as *L. monocytogenes* may engage in a nutrient battle against the host during infection. Thus, a vaccine developed against AdcA would likely be protective against many pathogenic streptococci. In conclusion, we have identified and delineated the roles of the major players in the arms race between GAS and the host for zinc, and demonstrated the translational potential of this signaling pathway for development of an effective GAS vaccine.

Funding Sources

This work was supported in part by the National Institute of Health grant (1R01AI109096-01A1 to M.K and GM059323 to J.D.H).

Conflict of Interest Statement

M.K has initiated a patent application on the utility of AdcA-NTD as a GAS vaccine. The authors declare no additional competing financial interests.

Author Contributions

N.M., K.N., M.G., R.J.O., and M.K. performed *in vitro* and *in vivo* experiments; N.M., H.D., and M.K., performed protein purification, crystallization, data collection, structure determination, and structural analyses; P.C., and J.D.H. carried out the ICP-MS metal content experiments and analyzed the data; N.M., H.D., and M.K. wrote the manuscript; M.K. designed and supervised the study; R.J.O., J.D.H., and M.K. edited the manuscript.

Acknowledgments

The authors acknowledge the staff of the 8.3.1 beam line at the Advanced Light Source for their assistance in data collection. Advanced Light Source was supported by Department of Energy contract DE-AC03-76SF00098. The coordinates and structure factors for the AdcR structure have been deposited in the protein data bank (PDB) with the accession codes 5JLS and 5JLU.

Appendix A. Supplementary data

Supplementary data to this article can be found online at http://dx.doi.org/10.1016/j.ebiom.2017.05.030.

References

Achouiti, A., Vogl, T., Endeman, H., Mortensen, B.L., Laterre, P.-F., Wittebole, X., van Zoelen, M.A.D., Zhang, Y., Hoogerwerf, J.J., Florquin, S., et al., 2014. Myeloid-related protein-8/14 facilitates bacterial growth during pneumococcal pneumonia. Thorax 69, 1034–1042.

Ammendola, S., Pasquali, P., Pistoia, C., Petrucci, P., Petrarca, P., Rotilio, G., Battistoni, A., 2007. High-affinity Zn2+ uptake system ZnuABC is required for bacterial zinc homeostasis in intracellular environments and contributes to the virulence of *Salmonella enterica*. Infect. Immun. 75, 5867–5876.

Bayle, L., Chimalapati, S., Schoehn, G., Brown, J., Vernet, T., 2011. Low, and Durmort, C. Zinc uptake by *Streptococcus pneumoniae* depends on both AdcA and AdcAII and is essential for normal bacterial morphology and virulence. Mol. Microbiol. 82, 904–916.

Beres, S.B., Carroll, R.K., Shea, P.R., Sitkiewicz, I., Martinez-Gutierrez, J.C., Low, D.E., McGeer, A., Willey, B.M., Green, K., Tyrrell, G.J., et al., 2010. Molecular complexity of successive bacterial epidemics deconvoluted by comparative pathogenomics. Proc. Natl. Acad. Sci. U. S. A. 107, 4371–4376.

Blencowe, D.K., Morby, A.P., 2003. Zn(II) metabolism in prokaryotes. FEMS Microbiol. Rev. 27, 291–311.

Botella, H., Peyron, P., Levillain, F., Poincloux, R., Poquet, Y., Brandli, I., Wang, C., Tailleux, L., Tilleul, S., Charriere, G.M., et al., 2011. Mycobacterial P(1)-type ATPases mediate resistance to zinc poisoning in human macrophages. Cell Host Microbe 10, 248–259.

Brenot, A., Weston, B.F., Caparon, M.G., 2007. A PerR-regulated metal transporter (PmtA) is an interface between oxidative stress and metal homeostasis in *Streptococcus pyogenes*. Mol. Microbiol. 63, 1185–1196.

Campoy, S., Jara, M., Busquets, N., Perez De Rozas, A.M., Badiola, I., Barbe, J., 2002. Role of the high-affinity zinc uptake *znuABC* system in *Salmonella enterica* serovar typhimurium virulence. Infect. Immun. 70, 4721–4725.

Carapetis, J.R., Beaton, A., Cunningham, M.W., Guilherme, L., Karthikeyan, G., Mayosi, B.M., Sable, C., Steer, A., Wilson, N., Wyber, R., et al., 2016. Acute rheumatic fever and rheumatic heart disease. Nat. Rev. Dis. Primers. 2, 15084.

Carapetis, J.R., Steer, A.C., Mulholland, E.K., Weber, M., 2005. The global burden of group A streptococcal diseases. Lancet Infect. Dis. 5, 685–694.

Coleman, J.E., 1998. Zinc enzymes. Curr. Opin. Chem. Biol. 2, 222–234.

Corbin, B.D., Seeley, E.H., Raab, A., Feldmann, J., Miller, M.R., Torres, V.J., Anderson, K.L., Dattilo, B.M., Dunman, P.M., Gerads, R., et al., 2008. Metal chelation and inhibition of bacterial growth in tissue abscesses. Science 319, 962–965.

Cunningham, M.W., 2000. Pathogenesis of group a streptococcal infections. Clin. Microbiol. Rev. 13, 470–511.

Dale, J.B., Niedermeyer, S.E., Agbaosi, T., Hysmith, N.D., Penfound, T.A., Hohn, C.M., Pullen, M., Bright, M.I., Murrell, D.S., Shenep, L.E., et al., 2015. Protective immunogenicity of group a streptococcal M-related proteins. Clin. Vaccine Immunol. 22, 344–350.

Damo, S.M., Kehl-Fie, T.E., Sugitani, N., Holt, M.E., Rathi, S., Murphy, W.J., Zhang, Y., Betz, C., Hench, L., Fritz, G., et al., 2013. Molecular basis for manganese sequestration by calprotectin and roles in the innate immune response to invading bacterial pathogens. Proc. Natl. Acad. Sci. U. S. A. 110, 3841–3846.

Davis, L.M., Kakuda, T., DiRita, V.J., 2009. A *Campylobacter jejuni znuA* orthologue is essential for growth in low-zinc environments and chick colonization. J. Bacteriol. 191, 1631–1640.

De Filippo, K., Neil, D.R., Mathies, M., Bangert, M., McNeill, E., Kadioglu, A., Hogg, N., 2014. A new protective role for S100A9 in regulation of neutrophil recruitment during invasive pneumococcal pneumonia. FASEB J. 28, 3600–3608.

Diaz-Ochoa, V.E., Lam, D., Lee, C.S., Klaus, S., Behnsen, J., Liu, J.Z., Chim, N., Nuccio, S.P., Rathi, S.G., Mastroianni, J.R., et al., 2016. Salmonella mitigates oxidative stress and thrives in the inflamed gut by evading calprotectin-mediated manganese sequestration. Cell Host Microbe 19, 814–825.

Gaddy, J.A., Radin, J.N., Loh, J.T., Piazuelo, M.B., Kehl-Fie, T.E., Delgado, A.G., Ilca, F.T., Peek, R.M., Cover, T.L., Chazin, W.J., et al., 2014. The host protein calprotectin modulates the *Helicobacter pylori cag* type IV secretion system via zinc sequestration. PLoS Pathog. 10, e1004450.

Garcia, Y.M., Barwinska-Sendra, A., Tarrant, E., Skaar, E.P., Waldron, K.J., Kehl-Fie, T.E., 2017. A superoxide dismutase capable of functioning with iron or manganese promotes the resistance of *Staphylococcus aureus* to calprotectin and nutritional immunity. PLoS Pathog. 13 (1), e1006125.

Guerra, A.J., Dann 3rd, C.E., Giedroc, D.P., 2011. Crystal structure of the zinc-dependent MarR family transcriptional regulator AdcR in the Zn(II)-bound state. J. Am. Chem. Soc. 133, 19614–19617.

Haley, K.P., Delgado, A.G., Piazuelo, M.B., Mortensen, B.L., Correa, P., Damo, S.M., Chazin, W.J., Skaar, E.P., Gaddy, J.A., 2015. The human antimicrobial protein calgranulin C participates in control of *Helicobacter pylori* growth and regulation of virulence. Infect. Immun. 83, 2944–2956.

Hood, M.I., Mortensen, B.L., Moore, J.L., Zhang, Y., Kehl-Fie, T.E., Sugitani, N., Chazin, W.J., Caprioli, R.M., Skaar, E.P., 2012. Identification of an *Acinetobacter baumannii* zinc acquisition system that facilitates resistance to calprotectin-mediated zinc sequestration. PLoS Pathog. 8, e1003068.

Kapur, V., Maffei, J.T., Greer, R.S., Li, L.-L., Adams, G.J., Musser, J.M., 1994. Vaccination with streptococcal extracellular cysteine protease (interleukin-1β convertase) protects mice against challenge with heterologous group A streptococci. Microb. Pathog. 16, 443–450.

Kehl-Fie, T.E., Skaar, E.P., 2010. Nutritional immunity beyond iron: a role for manganese and zinc. Curr. Opin. Chem. Biol. 14, 218–224.

Kirvan, C.A., Galvin, J.E., Hilt, S., Kosanke, S., Cunningham, M.W., 2014. Identification of streptococcal M-protein cardiopathogenic epitopes in experimental autoimmune valvulitis. J. Cardiovasc. Transl. Res. 7, 172–181.

Klaus, H., 2005. Bacterial zinc uptake and regulators. Curr. Opin. Microbiol. 8, 196–202.

Liu, J.Z., Jellbauer, S., Poe, A.J., Ton, V., Pesciaroli, M., Kehl-Fie, T.E., Restrepo, N.A., Hosking, M.P., Edwards, R.A., Battistoni, A., et al., 2012. Zinc sequestration by the neutrophil

protein calprotectin enhances Salmonella growth in the inflamed gut. Cell Host Microbe 11, 227–239.
Lusitani, D., Malawista, S.E., Montgomery, R.R., 2003. Calprotectin, an abundant cytosolic protein from human polymorphonuclear leukocytes, inhibits the growth of *Borrelia burgdorferi*. Infect. Immun. 71, 4711–4716.
Ma, Z., Gabriel, S.E., Helmann, J.D., 2011. Sequential binding and sensing of Zn(II) by *Bacillus subtilis* Zur. Nucleic Acids Res. 39, 9130–9138.
Mason, W.J., Skaar, E.P., 2009. Assessing the contribution of heme-iron acquisition to *Staphylococcus aureus* pneumonia using computed tomography. PLoS One 4, e6668.
Maurice, J., 2013. Rheumatic heart disease back in the limelight. Lancet 382, 1085–1086.
McNamara, C., Zinkernagel, A.S., Macheboeuf, P., Cunningham, M.W., Nizet, V., Ghosh, P., 2008. Coiled-coil irregularities and instabilities in group a *Streptococcus* M1 are required for virulence. Science 319, 1405–1408.
Moore, C.M., Helmann, J.D., 2005. Metal ion homeostasis in *Bacillus subtilis*. Curr. Opin. Microbiol. 8, 188–195.
Moulin, P., Patron, K., Cano, C., Zorgani, M.A., Camiade, E., Borezée-Durant, E., Rosenau, A., Mereghetti, L., Hiron, A., 2016. The *Adc/Lmb* system mediates zinc acquisition in *Streptococcus agalactiae* and contributes to bacterial growth and survival. J. Bacteriol. 198, 3265–3277.
Nakashige, T.G., Zhang, B., Krebs, C., Nolan, E.M., 2015. Human calprotectin is an iron-sequestering host-defense protein. Nat. Chem. Biol. 11, 765–771.
North, M., Steffen, J., Loguinov, A.V., Zimmerman, G.R., Vulpe, C.D., Eide, D.J., 2012. Genome-wide functional profiling identifies genes and processes important for zinc-limited growth of *Saccharomyces cerevisiae*. PLoS Genet. 8, e1002699.
Olsen, R.J., Shelburne, S.A., Musser, J.M., 2009. Molecular mechanisms underlying group a streptococcal pathogenesis. Cell. Microbiol. 11, 1–12.
Ong, C.L., Gillen, C.M., Barnett, T.C., Walker, M.J., McEwan, A.G., 2014. An antimicrobial role for zinc in innate immune defense against group A *streptococcus*. J Infect Dis 209, 1500–1508.
Porcheron, G., Schouler, C., Dozois, C.M., 2016. Survival games at the dinner table: regulation of Enterobacterial virulence through nutrient sensing and acquisition. Curr. Opin. Microbiol. 30, 98–106.
Reyes-Caballero, H., Guerra, A.J., Jacobsen, F.E., Kazmierczak, K.M., Cowart, D., Koppolu, U.M., Scott, R.A., Winkler, M.E., Giedroc, D.P., 2010. The metalloregulatory zinc site in *Streptococcus pneumoniae* AdcR, a zinc-activated MarR family repressor. J. Mol. Biol. 403, 197–216.
Rodriguez-Iturbe, B., Batsford, S., 2007. Pathogenesis of poststreptococcal glomerulonephritis a century after Clemens von Pirquet. Kidney Int. 71, 1094–1104.
Sabri, M., Houle, S., Dozois, C.M., 2009. Roles of the extraintestinal pathogenic *Escherichia coli* ZnuACB and ZupT zinc transporters during urinary tract infection. Infect. Immun. 77, 1155–1164.
Sanson, M., Makthal, N., Flores, A.R., Olsen, R.J., Musser, J.M., Kumaraswami, M., 2015. Adhesin competence repressor (AdcR) from *Streptococcus pyogenes* controls adaptive responses to zinc limitation and contributes to virulence. Nucleic Acids Res. 43, 418–432.
Sheel, M., Moreland, N.J., Fraser, J.D., Carapetis, J., 2016. Development of group a streptococcal vaccines: an unmet global health need. Expert Rev. Vaccines. 15, 227–238.
Shin, J.H., Jung, H.J., An, Y.J., Cho, Y.B., Cha, S.S., Roe, J.H., 2011. Graded expression of zinc-responsive genes through two regulatory zinc-binding sites in Zur. Proc. Natl. Acad. Sci. U. S. A. 108, 5045–5050.
Shin, J.H., Helmann, J.D., 2016. Molecular logic of the Zur-regulated zinc deprivation response in *Bacillus subtilis*. Nat. Commun. 7, 12612.
Sohnle, P.G., Collins-Lech, C., Wiessner, J.H., 1991. Antimicrobial activity of an abundant calcium-binding protein in the cytoplasm of human neutrophils. J Infect Dis 163, 187–192.
Steer, A.C., Carapetis, J.R., Dale, J.B., Fraser, J.D., Good, M.F., Guilherme, L., Moreland, N.J., Mulholland, E.K., Schodel, F., Smeesters, P.R., 2016. Status of research and development of vaccines for *Streptococcus pyogenes*. Vaccine 34, 2953–2958.
Steer, A.C., Dale, J.B., Carapetis, J.R., 2013. Progress toward a global group a streptococcal vaccine. Pediatr. Infect. Dis. J. 32, 180–182.
Tedde, V., Rosini, R., Galeotti, C.L., 2016. Zn2+ uptake in *Streptococcus pyogenes*: characterization of *adcA* and *lmb* null mutants. PLoS One 11, e0152835.
Urban, C.F., Ermert, D., Schmid, M., Abu-Abed, U., Goosmann, C., Nacken, W., Brinkmann, V., Jungblut, P.R., Zychlinsky, A., 2009. Neutrophil extracellular traps contain calprotectin, a cytosolic protein complex involved in host defense against *Candida albicans*. PLoS Pathog. 5, e1000639.
van Sorge, Nina M., Cole, Jason N., Kuipers, K., Henningham, A., Aziz, Ramy K., Kasirer-Friede, A., Lin, L., Berends, Evelien T.M., Davies, Mark R., Dougan, G., et al., 2014. The classical lancefield antigen of group a *Streptococcus* is a virulence determinant with implications for vaccine design. Cell Host Microbe 15, 729–740.
Wu, C.Y., Bird, A.J., Chung, L.M., Newton, M.A., Winge, D.R., Eide, D.J., 2008. Differential control of Zap1-regulated genes in response to zinc deficiency in *Saccharomyces cerevisiae*. BMC Genomics 9, 370.
Zhang, S., Green, N.M., Sitkiewicz, I., LeFebvre, R.B., Musser, J.M., 2006. Identification and characterization of an antigen I/II family protein produced by group a *Streptococcus*. Infect. Immun. 74, 4200–4213.